Numerical simulation using
vorticity-vector potential formulation

By H. Tokunaga

1. Motivation and objectives

An accurate and efficient computational method is needed for three-dimensional incompressible viscous flows in engineering applications. On solving the turbulent shear flows directly or using the subgrid scale model, it is indispensable to resolve the small scale fluid motions as well as the large scale motions. From this point of view, the pseudo-spectral method is used so far as the computational method. However, the finite difference or the finite element methods are widely applied for computing the flow with practical importance since these methods are easily applied to the flows with complex geometric configurations. However, there exist several problems on applying the finite difference method to direct and large eddy simulations.

Accuracy is one of most important problems. This point has been already addressed by the present author on the direct simulations on the instability of the plane Poiseuille flow and also on the transition to turbulence (Tokunaga, Ichinose & Satofuka, 1991a, b). In order to obtain high efficiency, the multi-grid Poisson solver is combined with the higher order accurate finite difference method (Tokunaga, Satofuka & Miyagawa, 1986).

The formulation method is also one of the most important problems in applying the finite difference method to the incompressible turbulent flows. The three-dimensional Navier-Stokes equations have been solved so far in the primitive variables formulation. One of the major difficulties of this method is the rigorous satisfaction of the equation of continuity. In general, the staggered grid is used for the satisfaction of the solenoidal condition for the velocity field at the wall boundary. However, the velocity field satisfies the equation of continuity automatically in the vorticity-vector potential formulation. From this point of view, the vorticity-vector potential method was extended to the generalized coordinate system (Tokunaga, Yoyeda & Satofuka, 1991). In the present article, we adopt the vorticity-vector potential formulation, the generalized coordinate system, and the 4th-order accurate difference method as the computational method. At first, we present the computational method and apply the present method to computations of flows in a square cavity at large Reynolds number in order to investigate its effectiveness.

As is well known, the major drawback of the vorticity vector potential formulation is in the difficulty of specifying the boundary condition in the multiply connected domain. In applying the vorticity vector potential formulation to the flow with the complex geometric configuration, for example the flow along the multi-airfoil, we have to clear this hurdle. As the next step, therefore, we extend the present computational method to calculate the flow in a multiply connected domain. Lastly, the formulation of LES is dealt with in the framework of the present computational method.

2. Accomplishments

2.1 Vorticity vector potential formulation

Three-dimensional motions of fluid are governed by the Navier-Stokes equations and the equation of continuity

$$\frac{\partial u_i}{\partial t} + (\mathbf{u} \bullet \nabla) u_i = -\nabla p + \frac{1}{Re} \Delta u_i, (i = x, y, z) \tag{1}$$

$$\nabla \bullet \mathbf{u} = 0. \tag{2}$$

where $\mathbf{u} = (u_x, u_y, u_z)$ denotes the velocity, p the pressure, Re the Reynolds number, ∇ the gradient operator, and Δ the Laplacian operator. Now we introduce the vorticity ω, the vector potential ψ, and the scalar potential ϕ as

$$\mathbf{u} = \nabla \times \psi + \nabla \phi \tag{3}$$

$$\omega = \nabla \times \mathbf{u} \tag{4}$$

Then, the Laplace equation for the scalar potential, the vorticity transport equations, and the Poisson equations for the vector potential are derived:

$$\Delta \phi = 0 \tag{5}$$

$$\frac{\partial \omega_i}{\partial t} + \frac{\partial}{\partial x_j}(u_j \omega_i) = \omega_j \frac{\partial u_i}{\partial x_j} + \frac{1}{Re} \frac{\partial^2 \omega_i}{\partial x_j^2} \tag{6}$$

$$\Delta \psi_i = -\omega_i \tag{7}$$

We introduce the generalized coordinate as

$$x = x(\xi, \eta), y = y(\xi, \eta), z = z(\zeta) \tag{8}$$

The partial differentiation operator is then transformed into

$$\frac{\partial}{\partial x} = \frac{1}{J}\left(\frac{\partial y}{\partial \eta}\frac{\partial}{\partial \xi} - \frac{\partial y}{\partial \xi}\frac{\partial}{\partial \eta}\right)$$

$$\frac{\partial}{\partial y} = \frac{1}{J}\left(\frac{\partial x}{\partial \xi}\frac{\partial}{\partial \eta} - \frac{\partial x}{\partial \eta}\frac{\partial}{\partial \xi}\right) \tag{9}$$

$$J = \frac{\partial x}{\partial \xi}\frac{\partial y}{\partial \eta} - \frac{\partial x}{\partial \eta}\frac{\partial y}{\partial \xi}$$

In order to specify the wall boundary condition, we define the the normal and the tangential component of ψ as

$$\psi_n = \mathbf{n} \bullet \psi, \psi_{\tau_1} = \tau_1 \bullet \psi, \psi_{\tau_2} = \tau_2 \bullet \psi \qquad (10)$$

where $\mathbf{n}$, τ_1, and τ_2 denote the normal and the tangential unit vector on the wall. Then, the wall boundary conditions for the vector potential are given as

$$\frac{\partial \psi_n}{\partial n} = \psi_{\tau_1} = \psi_{\tau_2} = 0 \qquad (11)$$

On the other hand, the boundary vorticity is calculated from its definition

$$\omega = \nabla \times \mathbf{u} \qquad (12)$$

2.2 Computational method

The explicit method of lines is adopted as the computational method. In this method, spatial discretizations and the time integration are treated separately. For spatial discretization, the 2nd- and 4th-order accurate modified differential quadrature (MDQ) method is used. Partial derivatives of ω, for example, are approximated as

$$\left.\frac{\partial \omega}{\partial \xi}\right|_{i,j,k} = \sum_{l=-L}^{L} a_{i,l} \omega_{i+l,j,k} \qquad (13)$$

$$\left.\frac{\partial^2 \omega}{\partial \xi^2}\right|_{i,j,k} = \sum_{l=-L}^{L} b_{i,l} \omega_{i+l,j,k}, \quad b_{i,l} = \sum_{m=-L}^{L} a_{i,m} a_{m,l} \qquad (14)$$

The 2nd-order accuracy is obtained by $L = 1$ and the 4th-order accuracy by $L = 2$. Derivatives in the η- and ζ-direction are approximated in the same manner. After the above spatial discretization, the vorticity transport equations are reduced to a set of ordinary differential equations (ODEs)

$$\frac{\mathrm{d}\vec{\omega}}{\mathrm{d}t} = \vec{F}(\vec{\omega}) \qquad (15)$$

$$\vec{\omega} = (\omega_{x,2,2,2}, \omega_{x,3,2,2}, \ldots, \omega_{z,I-1,J-1,K-1})^T \qquad (16)$$

where I, J, and K represent the grid number in the ξ-, η-, and ζ-direction, respectively. As a time integration scheme of a set of ODEs, we apply the Runge-Kutta-Gill method.

2.3 Computation of flows in a square cavity

In order to confirm effectivity of the present computational method, we first carry out simulations of flows in a square cavity at Reynolds numbers $Re = 10^3$ and 10^4. Figure 1 shows the velocity distribution on centerlines of the cavity. It is shown
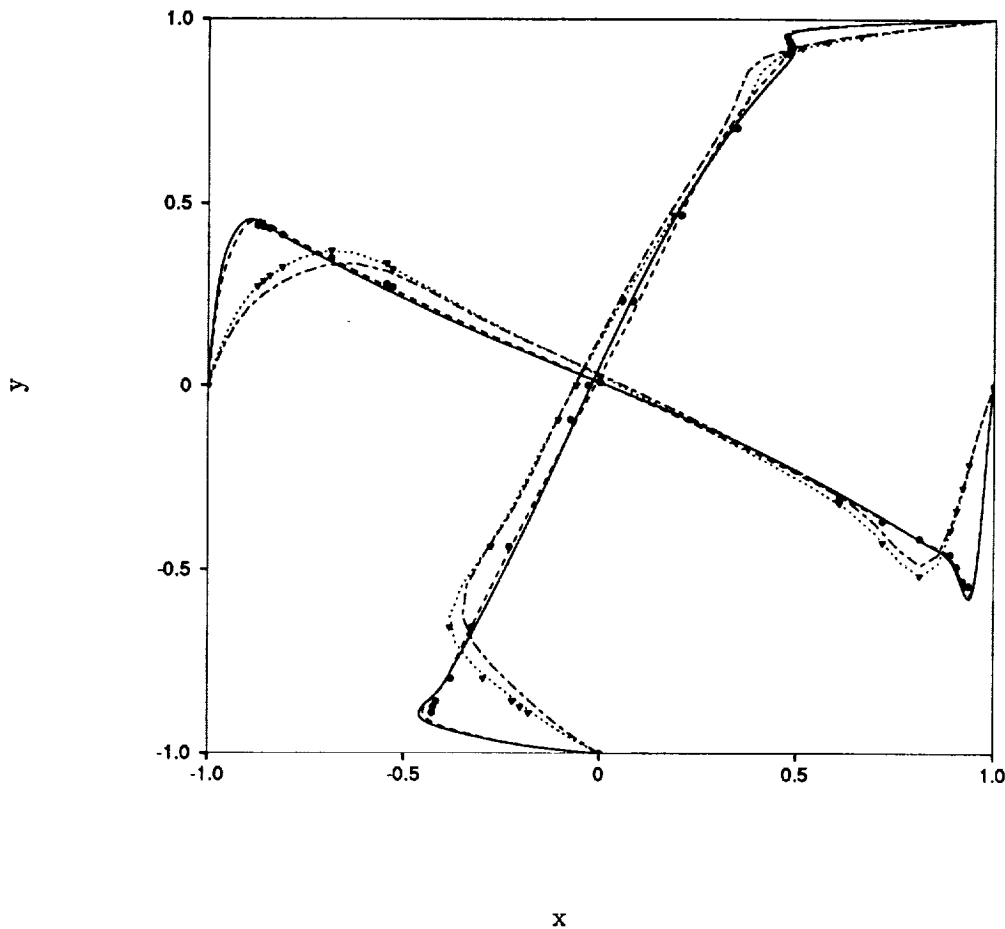
FIGURE 1.   Velocity distribution of the flow in a square cavity at $Re = 10^3$ and 10^4. Chain dot and chain dash line depict the result by the 4th- and 2nd-order method at $Re = 10^3$ respectively; solid and dash line represent the result by the 4th- and 2nd-order method at $Re = 10^4$ respectively. Triangle and circle depict the results by Ghia *et al.*

that the result of the 4th-order accurate method with the less grid points (65×65 at $Re = 10^3$) is in good agreement with that of Ghia et al.(1982).

In computation of the cavity flow at $Re = 10^4$, we need the grid points 129×129 in order to make the grid sufficiently dense in the vicinity of the wall. Figure 2 shows the convergence history of these computations with 2nd- and 4th-order accuracy. We needed 75000 time steps with $\Delta t = 1/125$ in order to obtain the converged solution when we used the 2nd-order accurate method. It is shown that the residual

oscillates drastically in time, and a great number of time steps are needed to attain the converged solution even for the 2nd-order method. However, the result with the 4th-order accuracy shows that the L_2 residual preserves the constant level even at $t = 900$, and, therefore, it is concluded that the flow is unsteady.
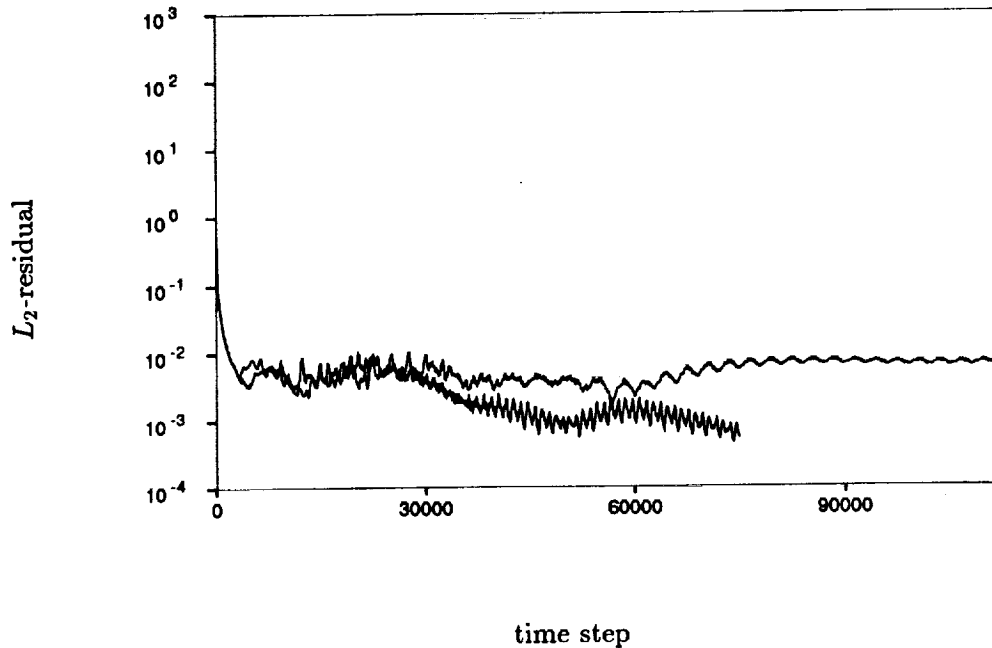

FIGURE 2.   Convergence history of the cavity flow at $Re = 10^4$.

In order to investigate the temporal behavior of the flow, we show the vorticity contours at the early stage $t = 50$, 60, and 70, the middle stage $t = 140$, 150, and 160, and the later stage $t = 240$, 250, and 260. Since the present result has a fourth-order accuracy not only for the spatial discretization but also for time discretization, we can see the actual development of the cavity flow from the initial state in which the fluid is at rest.

At an early stage, we find that there exists a number of vortices and that they are stretched in the course of time. The main vortex grows near the center of the cavity, and the other vortices are moved by rotation of the main flow. The stretching is caused by this main flow. However, the center of the main vortex is displaced by the mutual interaction of vortices.

In the middle stage, we find that the main vortex is enclosed by the additional elongated vortex with the same sign. It is well known that a pair of vortices with the same sign rotate around each other along the weighting center of the pair. Thus, the unsteady motion of fluid is sustained. The center of the main vortex moves rapidly.
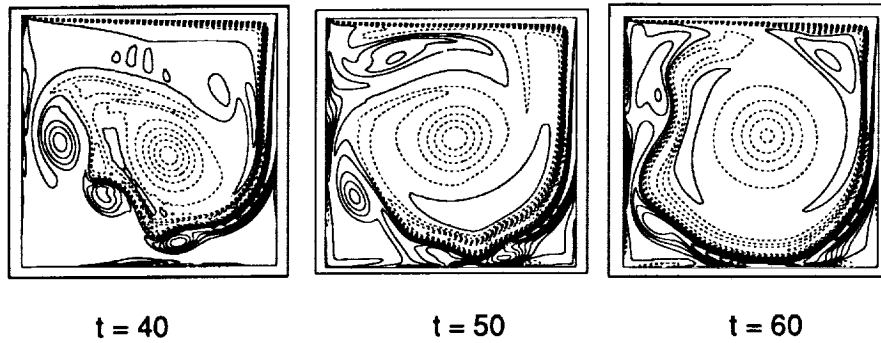
FIGURE 3.   Vorticity contours of the cavity flow at $Re = 10^4$ at early time stage.
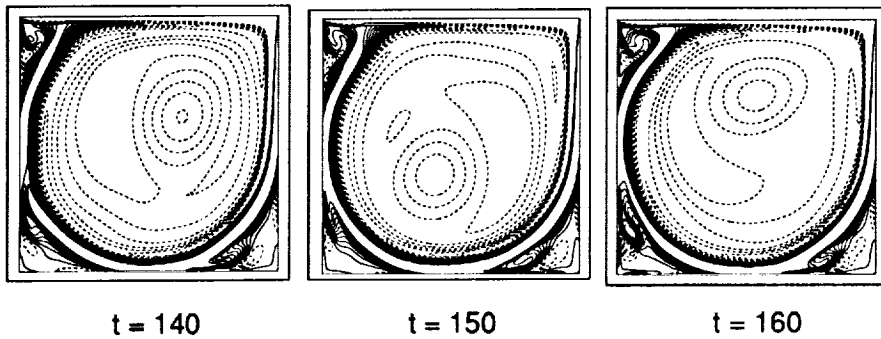

FIGURE 4.   Vorticity contours of the cavity flow at $Re = 10^4$ at middle time stage.

The Biot-Savart velocity induced by the vortex is long-range, so the structure of small vortices in the corners of the cavity changes significantly in the course of time.

The pair of vortices persist even at the later stage. However, at $t = 260$, the neighboring vortex is absorbed by the main vortex. Figure 6 shows the vorticity contours at $t = 840$ and 850. The vortex sheets are extremely stretched, and one of them is cut. The vortex generated by this mechanism interacts with other vortices, which explains the unsteadiness of the flow in a cavity at high Reynolds number.

2.4 Computation of flows in a multiply connected domain

In general, the stream function value on the multiply connected domain is not known *a priori*. In order to resolve this problem, we apply the constraint proposed by Girault and Rivart (1979)
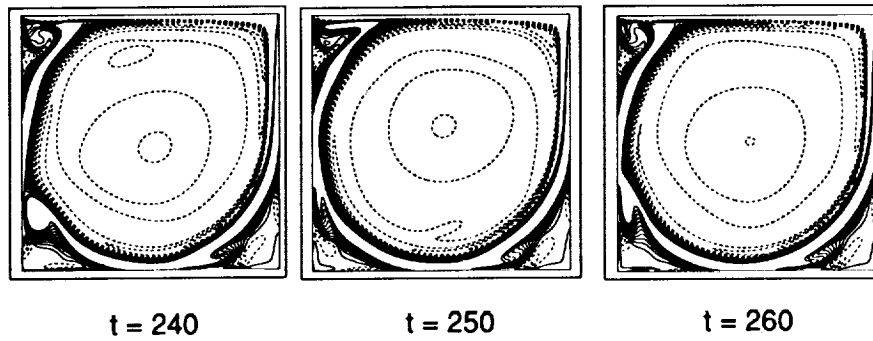
t = 240   t = 250   t = 260

FIGURE 5.   Vorticity contours of the cavity flow at $Re = 10^4$ at later time stage.

t = 840   t = 850
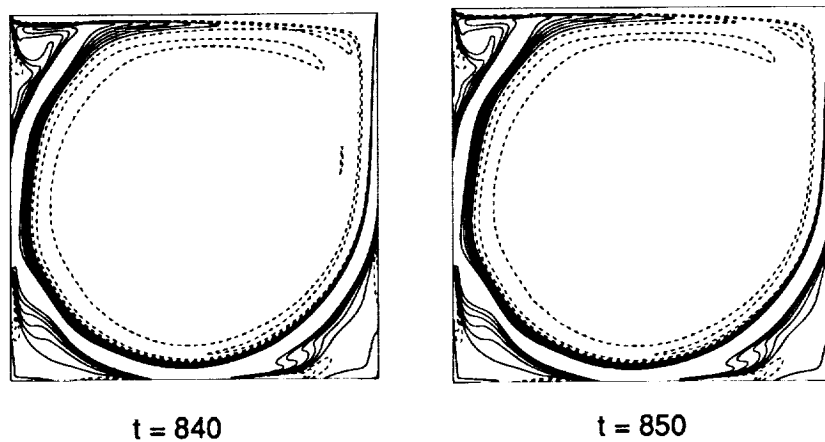
FIGURE 6.   Vorticity contours of the cavity flow at $Re = 10^4$ at the latest time stage.

$$\oint_\Gamma \frac{\partial \omega}{\partial n} \mathrm{d}s = 0 \tag{17}$$

where Γ denotes the surface of the body placed in the flow. In the present computation, the integral constraint is applied when the Poisson equation on the stream function is solved. We depict the stream line in Figure 7. The stream function value is specified to 1 on the upper wall and 0 on the lower wall. We ultimately obtained the stream function value -0.11375 on the square, which shows a good agreement with the result of Lippke and Wagner (1991).
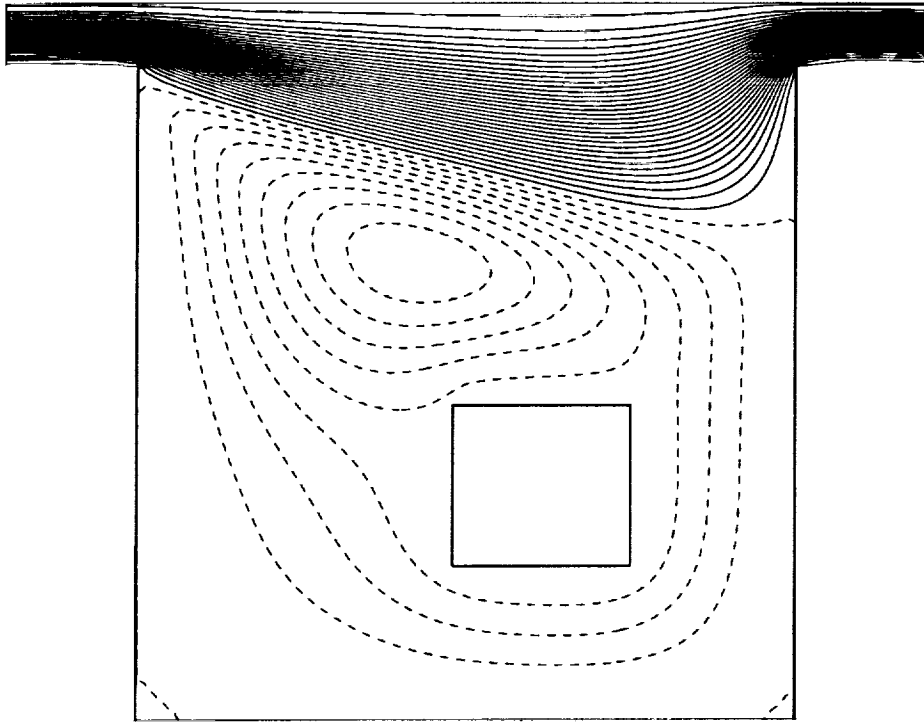
FIGURE 7. Streamline lines of the flow in a multiply connected domain at $Re = 20$.

2.5 Computation of transition of channel flow using LES

For the subgrid-scale model, we choose the dynamical model proposed by Germano *et al.* (1991). Then, the basic equation of LES is obtained in the vorticity vector potential formulation as

$$\frac{\partial \bar{\omega}_1}{\partial t} + \frac{\partial}{\partial x_j}(\bar{u}_j\bar{\omega}_1) = \bar{\omega}_j\frac{\partial \bar{u}_1}{\partial x_j} + \left(\frac{\partial^2 \nu_t}{\partial x_2 \partial x_j}\bar{S}_{3j} - \frac{\partial^2 \nu_t}{\partial x_3 \partial x_j}\bar{S}_{2j}\right) +$$
$$\frac{1}{2}\left(\frac{\partial \nu_t}{\partial x_2}\frac{\partial^2 \bar{u}_3}{\partial x_j^2} - \frac{\partial \nu_t}{\partial x_3}\frac{\partial^2 \bar{u}_2}{\partial x_j^2}\right) + \frac{1}{2}\frac{\partial \nu_t}{\partial x_j}\frac{\partial \bar{\omega}_1}{\partial x_j} + (\frac{1}{2}\nu_t + \frac{1}{Re})\frac{\partial^2 \bar{\omega}_1}{\partial x_j^2}$$

$$\frac{\partial \bar{\omega}_2}{\partial t} + \frac{\partial}{\partial x_j}(\bar{u}_j \bar{\omega}_2) = \bar{\omega}_j \frac{\partial \bar{u}_2}{\partial x_j} + \left(\frac{\partial^2 \nu_t}{\partial x_3 \partial x_j} \bar{S}_{1j} - \frac{\partial^2 \nu_t}{\partial x_1 \partial x_j} \bar{S}_{3j} \right) +$$

$$\frac{1}{2}\left(\frac{\partial \nu_t}{\partial x_3} \frac{\partial^2 \bar{u}_1}{\partial x_j^2} - \frac{\partial \nu_t}{\partial x_1} \frac{\partial^2 \bar{u}_3}{\partial x_j^2} \right) + \frac{1}{2}\frac{\partial \nu_t}{\partial x_j} \frac{\partial \bar{\omega}_2}{\partial x_j} + (\frac{1}{2}\nu_t + \frac{1}{Re})\frac{\partial^2 \bar{\omega}_i}{\partial x_j^2} \tag{18}$$

$$\frac{\partial \bar{\omega}_3}{\partial t} + \frac{\partial}{\partial x_j}(\bar{u}_j \bar{\omega}_3) = \bar{\omega}_j \frac{\partial \bar{u}_3}{\partial x_j} + \left(\frac{\partial^2 \nu_t}{\partial x_1 \partial x_j} \bar{S}_{2j} - \frac{\partial^2 \nu_t}{\partial x_2 \partial x_j} \bar{S}_{1j} \right) +$$

$$\frac{1}{2}\left(\frac{\partial \nu_t}{\partial x_1} \frac{\partial^2 \bar{u}_2}{\partial x_j^2} - \frac{\partial \nu_t}{\partial x_2} \frac{\partial^2 \bar{u}_1}{\partial x_j^2} \right) + \frac{1}{2}\frac{\partial \nu_t}{\partial x_j} \frac{\partial \bar{\omega}_3}{\partial x_j} + (\frac{1}{2}\nu_t + \frac{1}{Re})\frac{\partial^2 \bar{\omega}_3}{\partial x_j^2}$$

where ν_t denotes the dynamical subgrid scale turbulent viscosity and $\bar{S}_{i,j}$ the strain tensor. The generalized coordinate transformation is applied to this equation.

At first we will carry out LES of a transition of plane channel flow in order to investigate the validity of the present method. The initial condition is created by using the result of the direct simulation of 2-D and 3-D linear instability (Tokunaga, Satofuka & Miyagawa, 1986)

3. Summary and future plans

An accurate and efficient computational method is presented for incompressible viscous flows. It is shown that the present method well predicts the flow in multiply connected domain. The 4th-order accurate method shows that the square cavity flow can be calculated accurately by less grid points in comparison with the 2nd-order method at $Re = 10^3$. Further, it is shown that the cavity flow is unsteady at $Re = 10^4$, and actual process of the flow development is cleared by using the 4th-order accurate method.

The next step in this work will be to test the large eddy simulation of transition in a plane channel dealt with by Germano *et al.* (1991), and this study is under way. The ultimate goal of this work is direct and large eddy simulation of the flows in a multiply connected domain, which is of practical importance in aerodynamics.

REFERENCES

GERMANO, G., PIOMELLI, U., MOIN, P. & CABOT, W. H. 1991 A dynamical subgrid-scale eddy viscosity model. *Phys. Fluids.* **A3**, 1760-1765.

GIRAULT, V. & RAVIART, P. A. 1979 Finite element approximation of Navier-Stokes equations. *Lecture Notes in Mathematics.* **749**, Springer-Verlag.

GHIA, U., GHIA, K. N. & SHIN, T. 1982 High-Re solutions for incompressible flow using the Navier-Stokes equations and a multi-grid method. *J. Comp. Phys.* **48**, 387-411.

LIPPKE, A. & WAGNER, H. 1991 Numerical solution of the Navier-Stokes equation in multiply connected domains. *Computers & Fluids.* **20**, 19-28.

TOKUNAGA, H., ICHINOSE, K. & SATOFUKA, N. 1991a Numerical simulation of transient turbulent flows by the vorticity-vector potential formulation. *Computers & Fluids.* **19**, 413-420.

TOKUNAGA, H., ICHINOSE, K. & SATOFUKA, N. 1991b Direct simulation of transient turbulent flows using generalized method of lines. *Advances in Numerical Simulation of Turbulent Flows, ASME FED.* **117**, 57-82.

TOKUNAGA, H., SATOFUKA, N. & MIYAGAWA, H. 1986 Direct simulations of shear flow turbulence in a plane channel by sixth order accurate method of lines with new sixth order accurate multi-grid Poisson solver. *Lecture Notes in Physics.* **264**, Springer-Verlag.

TOKUNAGA, H., SATOFUKA, N. & MIYAGAWA, H. 1986 Direct simulation on instability of the plane Poiseuille flow. *Memoirs of Faculty of Engineering and Design, Kyoto Institute of Technology.* **34**, 72.

TOKUNAGA, H., SATOFUKA, N. & YOSHIKAWA, T. 1987 Direct simulation of high Reynolds number flows using a new integer-differential solver. *AIAA-87-1175-CP.*

TOKUNAGA, H., YOYEDA, K. & SATOFUKA, N. 1991 Direct simulation of three-dimensional flows using generalized vector potential method. *AIAA-91-1610-CP.*